High-throughput screening of strong electron-phonon couplings in ternary metal diborides

Renhai Wang[1], Yang Sun[2,3*], Feng Zhang[2,4], Feng Zheng[5], Yimei Fang[5], Shunqing Wu[5], Huafeng Dong[1*], Cai-Zhuang Wang[2,4], Vladimir Antropov[2,4], and Kai-Ming Ho[2]

[1]*School of Physics and Optoelectronic Engineering, Guangdong University of Technology, Guangzhou 510006, China*
[2]*Department of Physics, Iowa State University, Ames, Iowa 50011, USA*
[3]*Department of Applied Physics and Applied Mathematics, Columbia University, New York, NY, 10027, USA*
[4]*Ames Laboratory, U.S. Department of Energy, Ames, Iowa 50011, USA*
[5]*Department of Physics, Xiamen University, Xiamen 361005, China*

[*]Email: yangsun@iastate.edu or hfdong@gdut.edu.cn

Abstract

We perform a high-throughput screening on phonon-mediated superconductivity in ternary metal diboride structure with alkali, alkaline earth, and transition metals. We find 17 ground states and 78 low-energy metastable phases. From fast calculations of zone-center electron-phonon coupling, 43 compounds are revealed to show electron-phonon coupling strength higher than that of MgB_2. An anti-correlation between energetic stability and electron-phonon coupling strength is identified. We suggest two phases, i.e., Li_3ZrB_8 and Ca_3YB_8, to be synthesized, which show reasonable energetic stability and superconducting critical temperature.

Keywords: Ternary metal diborides, High-throughput calculation, Material discovery, Superconductivity

I. Introduction

Superconductivity has irreplaceable applications in many fields such as energy, medical care, transportation, and quantum computing. The search for new superconductors with a high critical temperature (T_c) is always a major scientific task that can open the door to many future techniques. Since 2001, the discovery of remarkably high superconducting T_c in MgB_2 [1] has stimulated great interest in searching for phonon-mediated superconductors in the layered hexagonal metal diborides structures [2-9]. Many attempts have been made by doping other elements to increase T_c of MgB_2 [10-12], which include $Mg_{1-x}Li_xB_2$ [13], $Mg_{1-x}Zr_xB_2$ [14], $Mg_{1-x}Zn_xB_2$ [15], $Mg_{1-x}Nb_xB_2$ [16], $Mg_{1-x}Sc_xB_2$ [17], $Mg_{1-x}Ti_xB_2$ [18], $Mg_{1-x}Na_xB_2$ [15] and $Mg_{1-x}Ca_xB_2$ [15]. However, most experimental data show a decreasing trend of T_c with an increasing amount of doping metal. Other metal diborides phases without Mg have also been explored, such as ZrB_2 [19], NbB_2 [20] and TaB_2 [21]; however, they only showed vanishing T_c. Recent experiments identify MoB_2 [22] and WB_2 [23] showing high T_c while high pressures of greater than 50 GPa are required. First-principle calculations also demonstrated a few possibilities of high T_c in metal diborides. A well-known case is the CaB_2 [24], where the electron-phonon coupling (EPC) is much stronger than that in MgB_2. Unfortunately, it's difficult to synthesize due to inferior thermodynamic stability. Doping with Cd and Ba in MgB_2 is predicted to show higher T_c than MgB_2, but such doped structures are also difficult to be synthesized experimentally [25-26]. Therefore, the thermodynamic stability and superconducting properties should be considered simultaneously to find new experimentally feasible ternary superconductors in metal diborides.

While the dopants should be as diverse as possible, it is difficult to efficiently screen out promising superconductors among a large number of candidates with theoretical T_c calculations. This is mainly because the detailed calculation of the electron-phonon coupling from density-functional perturbation theory (DFPT) [27] is complicated and time-consuming. We recently found that single-cell frozen-phonon calculations of the EPC strength of the zone-center phonons can be an efficient alternative to full density functional theory (DFT) evaluation of the Eliashberg function [28]. It well distinguishes strong EPC in the MgB_2 and high-pressure hydride systems [28]. Therefore it can be a fast descriptor of the full Brillouin zone EPC constant for the metal diboride family. In this work, we employ this method to perform a fast screening of strong EPC on ternary metal diboride phases. A large number of substituted phases are screened based on energetical stability and zone-center EPC strength. The detailed full Brioullion zone calculations of EPC and T_c are performed for promising candidates.

II. Computational methods

The AlB_2-type primitive cell (space group: P6/mmm) was expanded by 1×1×2 or 2×2×1 to generate $M_{1-x}N_xB_2$ ternary metal diboride structures (M and N representing the metal elements). The ratio x includes 0.25 (M_3NB_8), 0.50 (MNB_4) and 0.75 (MN_3B_8). Within the limited cell size, we select all symmetry-inequivalent structures from the candidates, which generate one configuration for M_3NB_8 or MN_3B_8 and two for MNB_4 (see Supplementary Materials **Fig. S1** for details). The ternary structures are optimized by *ab initio* calculations, which were performed using the projector augmented wave (PAW) method [29] within density functional theory as implemented in the VASP code [30-31]. The exchange and correlation energy are treated without the spin-polarized generalized gradient approximation (GGA) and parameterized by the Perdew-Burke-Ernzerhof formula (PBE) [32]. A plane-wave basis was used with a kinetic energy cutoff of 520 eV, and the convergence criterion for the total energy was set to 10^{-5} eV. Monkhorst–Pack's sampling scheme [33] was adopted for Brillouin zone sampling with a k-point grid of $2\pi \times 0.033$ Å^{-1}. The lattice vectors (supercell shape and size) and atomic coordinates are fully relaxed until the force on each atom is less than 0.01 eV/Å.

The formation energy E_f of ternary $M_xN_yB_z$ is calculated by

$$E_f = \frac{E(M_xN_yB_z) - xE(M) - yE(N) - zE(B)}{x+y+z} \quad (1)$$

where $E(M_xN_yB_z)$ is the total energy of the $M_xN_yB_z$; $E(M)$, $E(N)$ and $E(B)$ are the total energy of M, N, and B ground-state bulk phases, respectively. To characterize the energetic stability of $M_xN_yB_z$, we calculated the formation energy differences with respect to the three reference phases, named $M_{x1}N_{y1}B_{z1}$, $M_{x2}N_{y2}B_{z2}$, and $M_{x3}N_{y3}B_{z3}$, forming the Gibbs triangle on the convex hull (denoted as E_d) are calculated. Considering $M_xN_yB_z \rightarrow \alpha M_{x1}N_{y1}B_{z1} + \beta M_{x2}N_{y2}B_{z2} + \gamma M_{x3}N_{y3}B_{z3}$, E_d can then be calculated as:

$$E_d = \frac{E_f(M_xN_yB_z) - \alpha E_f(M_{x1}N_{y1}B_{z1}) - \beta E_f(M_{x2}N_{y2}B_{z2}) - \gamma E_f(M_{x3}N_{y3}B_{z3})}{x+y+z} \quad (2)$$

If $E_d = 0$, it indicates the $M_xN_yB_z$ is a new ground state and the existing convex hull should be updated. The reference of convex hulls are obtained from the Material Project dataset [34].

The high-throughput screening of strong EPC in these metal borides is based on fast frozen-phonon

calculation of zone-center EPC strength [28], defined by

$$\lambda_{\Gamma} = \sum_{\nu} \lambda_{\Gamma\nu} \tag{3}$$

where $\sum_{\nu}$ indicates the summation of all modes at zone-center Γ. $\lambda_{\Gamma\nu}$ is defined by

$$\lambda_{\Gamma\nu} = \frac{\tilde{\omega}_{\Gamma\nu}^2 - \omega_{\Gamma\nu}^2}{4\omega_{\Gamma\nu}^2} \tag{4}$$

where the $\omega_{\Gamma\nu}$ and $\tilde{\omega}_{\Gamma\nu}$ are screened and unscreened phonon frequencies of mode ν at zone-center, respectively. The phonon frequencies were calculated with the single-cell and finite displacement method implemented in the Phonopy code [35]. The displacement amplitude in the frozen-phonon calculations is 0.02 Å. The convergence criterion of total energy is 10^{-8} eV.

The calculations of full Brillouin-zone EPC constants and T_c of MgB_2, Li_3ZrB_8, and Ca_3YB_8 were performed based on density-functional perturbation theory [27] implemented in Quantum ESPRESSO code [36-38] . We used the ultra-soft pseudopotentials from the GBRV library [39]. After the convergence test, the plane-wave cut-off and the charge density cut-off were chosen to be 60 and 500 Ry, respectively. The reference calculation of dynamical matrix and EPC matrix elements in MgB_2 is based on the AlB_2-type primitive cell. Self-consistent field (SCF) calculations were performed with a dense k mesh of 48×48×48, followed by the DFPT calculation with the k mesh of 24×24×24 and the q mesh of 6×6×6. The calculations of Li_3ZrB_8 and Ca_3YB_8 were based on the 2×2×1 supercell, using a dense k mesh of 24×24×48 for the SCF calculation and the k of 12×12×24 and the q mesh of 3×3×6 for DFPT calculations. The convergence threshold in DFPT calculations was 1×10^{-12} Ry. The gaussian smearing of width was 0.01 Ry.

The isotropic Eliashberg spectral function was obtained via the average over the Brillouin zone [40]

$$\alpha^2(\omega)F(\omega) = \frac{1}{2N(\epsilon_F)} \sum_{\boldsymbol{q}\nu} \frac{\gamma_{\boldsymbol{q}\nu}}{\hbar\omega_{\boldsymbol{q}\nu}} \delta(\omega - \omega_{\boldsymbol{q}\nu}) \tag{5}$$

where $N(\epsilon_F)$ is the density of states at the Fermi level ϵ_F; $\omega_{\boldsymbol{q}\nu}$ denotes the phonon frequency of mode ν with wave vector $\boldsymbol{q}$. $\gamma_{\boldsymbol{q}\nu}$ is the phonon linewidth defined by $\gamma_{\boldsymbol{q}\nu} = \frac{2\pi\omega_{\boldsymbol{q}\nu}}{\Omega_{BZ}} \sum_{ij} \int d^3k |g^{ij}_{\boldsymbol{k},\boldsymbol{q}\nu}|^2 \delta(\epsilon_{\boldsymbol{q},i} - \epsilon_F)\delta(\epsilon_{\boldsymbol{k}+\boldsymbol{q},j} - \epsilon_F)$, where $g^{ij}_{\boldsymbol{k},\boldsymbol{q}\nu}$ is the EPC matrix element; $\epsilon_{\boldsymbol{q},i}$ and $\epsilon_{\boldsymbol{k}+\boldsymbol{q},i}$ are eigenvalues of Kohn-Sham orbitals at bands i, j and wave vectors $\boldsymbol{q}$, $\boldsymbol{k}$. The full Brillouin-zone EPC constant λ is determined through the integration of the Eliashberg spectral function,

$$\lambda = 2\int \frac{\alpha^2(\omega)F(\omega)}{\omega} d\omega \tag{6}$$

The T_c is obtained with the analytical McMillan equation [41] modified by the Allen-Dynes [42-43]

$$T_c = \frac{\omega_{log}}{1.2} \exp\left[\frac{-1.04(1+\lambda)}{\lambda(1-0.62\mu^*) - \mu^*}\right] \tag{7}$$

where ω_{log} is the logarithmic average frequency $\omega_{log} = \exp\left[\frac{2}{\lambda}\int \frac{d\omega}{\omega}\alpha^2(\omega)F(\omega)log\omega\right]$; μ^* is the effective screened Coulomb repulsion constant, set as 0.1. While the estimation of T_c is done using 'single band' approach for this work, it is well known that the superconductivity in MgB_2 has multiband character [3, 9]. A corresponding multi-band modification of the McMillan formula can be applied with the Ref. [9]. We leave

these calculations of multiband superconductivity for the future.

III. Results and discussion

3.1 Binary metal diboride phases

We first examine the effect of metal substitution in the binary metal diboride structure with 12 elements including Ca, Cd, K, Na, Zn, Li, Nb, Y, Sc, Zr, Ti and Mg. The energetic stability is described by the energy above the convex hull E_d (see the method section for definition of E_d). The EPC strength is described with the zone-center EPC strength λ_Γ (see the method section for definition of λ_Γ). As shown in Fig. 1, Zr, Ti, Sc, Y, Nb diborides show good energetic stability but no EPC. Ca, Cd, K diborides show strong EPC but poor energetic stability. Overall, Fig. 1 shows an anti-correlation between E_d and λ_Γ that a stronger EPC (larger λ_Γ) leads to worse energetic stability (higher E_d). Interestingly, MgB_2 phase shows both a decent λ_Γ and strong energetic stability, which is an outlier from the general anti-correlation of the two properties. CaB_2 system shows the best EPC but poor energetic stability, making it difficult to synthesize in experiments [24]. Therefore the correlation in Fig. 1 is in line with the previous findings that substitution of Mg in MgB_2 either leads to lower T_c or reduced stability. This demonstrates that the λ_Γ provides a good description of EPC strength for metal diboride systems, consistent with a previous comparative study between MgB_2 and AlB_2 [28].

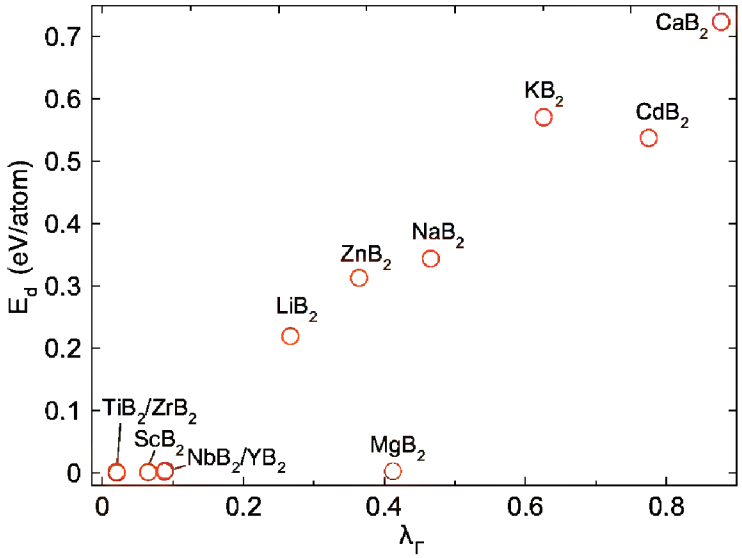

Figure 1 E_d-λ_Γ diagram of 12 binary MB_2 structures. Lower E_d indicates better stability. Higher λ_Γ indicates stronger EPC.

3.2 $M_{1-x}N_xB_2$ ternary convex hull

We calculate energetic stability and EPC strength in the ternary $M_{1-x}N_xB_2$ by mixing 12 metals on the metal sites in the supercell of the AlB_2 structure (see Method). The combination of M and N results in 66 (C_{12}^2) M-N-B ternary systems with 198 geometrically inequivalent structures containing three compositions, i.e., MNB_4, MN_3B_8 and M_3NB_8. The convex hull is constructed for each ternary phase to describe its energetic stability. Taking Nb-Sc-B as an example in Fig. 2, the compositional space (Gibbs triangle) is partitioned into multiple triangular pieces by the ground state structures, which form the corners of the convex hull for

the corresponding ternary system. The known stable ground states are obtained from the Materials Project (MP) [34] database. In Fig. 2(a), the known Na-Sc-B phases form a reference convex hull. If any new structure has formation energy below this convex hull surface, it is defined as a new ground state, and the convex hull surface is updated by including the new phase. In Fig. 2(b), three Nb-Sc-B structures ($ScNbB_4$, $ScNb_3B_8$, Sc_3NbB_8) are found to be the ground states phases, considerably modifying the original convex hull reference shown in Fig. 2(a).

In total, 17 ternary phases are identified as ground states, including $ScNbB_4$, $ScNb_3B_8$, Sc_3NbB_8, $LiNb_3B_8$, $CaNbB_4$, $YNbB_4$, $YZrB_4$, $ZrScB_4$, Zr_3ScB_8, $ZrNbB_4$, $ScTiB_4$, Mg_3ScB_8, $MgNbB_4$, $MgNb_3B_8$, Ti_3NbB_8, $TiNbB_4$ and $TiNb_3B_8$. Two of them, i.e., $TiNbB_4$ and $ZrNbB_4$, are previously reported in the MP database. Moreover, $Mg_{0.75}Sc_{0.25}B_2$ [17] and three $Zr_{1-x}Nb_xB_2$ ($x = 0.25$, 0.5, 0.75) were experimentally synthesized [44]. The convex hulls are updated by including the new ground states, shown in Supplementary Materials **Fig. S2**. Besides, we identify many low-energy metastable states that may be synthesizable by experiments, especially under non-equilibrium synthesis routes. For instance, recent experiments on LiNiB showed that the $Li_{0.75}[NiB]_2$ phase with E_d = 0.21 eV/atom can be synthesized from high-temperature reactions [45]. Metastable $SnTi_2N_4$ (E_d = 0.2 eV/atom) [46] and metastable $ZnMoN_2$ in a wurtzite-derived structure (E_d = 0.16 eV/atom) [47] are all successfully synthesized in experiments. Here, by using a threshold of $E_d < 0.2$ eV/atom, we identify 78 metastable metal diboride phases, which may have experimental synthesizability. The detailed information on these metastable phases is shown in Supplementary **Table S1**. We note that present work only considered the AlB_2 prototypical structure. From the computational point of view, to determine whether structures can be synthesized in practice, other crystal structures may also be considered. Crystal structure search with USPEX [48], CALYPSO [49], AGA [50-51], etc. can be applied for the system of interest in future.

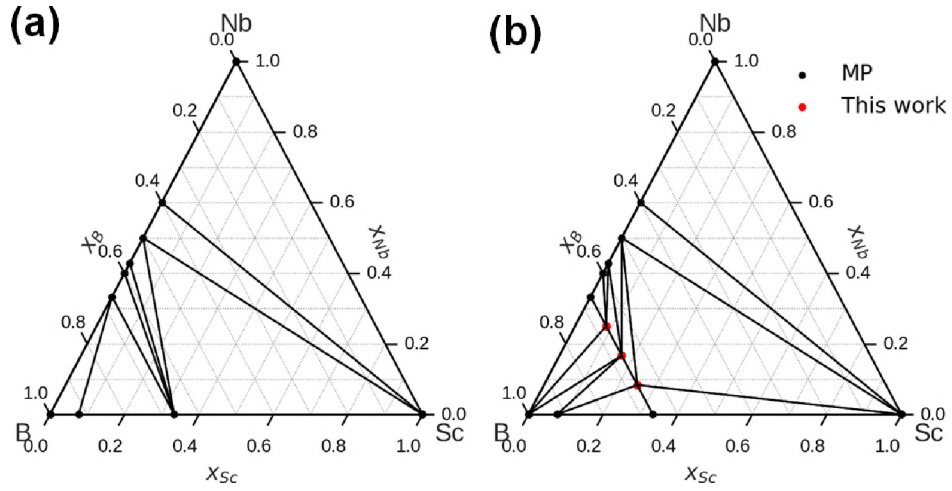

Figure 2 Convex hull of the Sc-Nb-B system. (a) Previously reported phases from MP database; (b) Convex hull including the $ScNbB_4$, $ScNb_3B_8$ and Sc_3NbB_8 phases. The black lines separate the compositional space to Gibbs triangles.

3.3 E_d-λ_Γ correlation in ternary $M_{1-x}N_xB_2$

To describe EPC, λ_Γ are computed for all ternary $M_{1-x}N_xB_2$. The maps of E_d and λ_Γ with all substituted

structures are shown in Fig. 3. The color of each grid indicates the E_d or λ value of the corresponding phases. The more bluish coding indicates better energetic stability or stronger EPC. The data of the binary phases are listed in the diagonal grids as reference. One can see the compounds containing Mg, Zr, Nb, Sc, Ti, and Y elements show better thermodynamic stability while those containing Mg, Li, Cd, Na, Ca and K have better EPC strength.

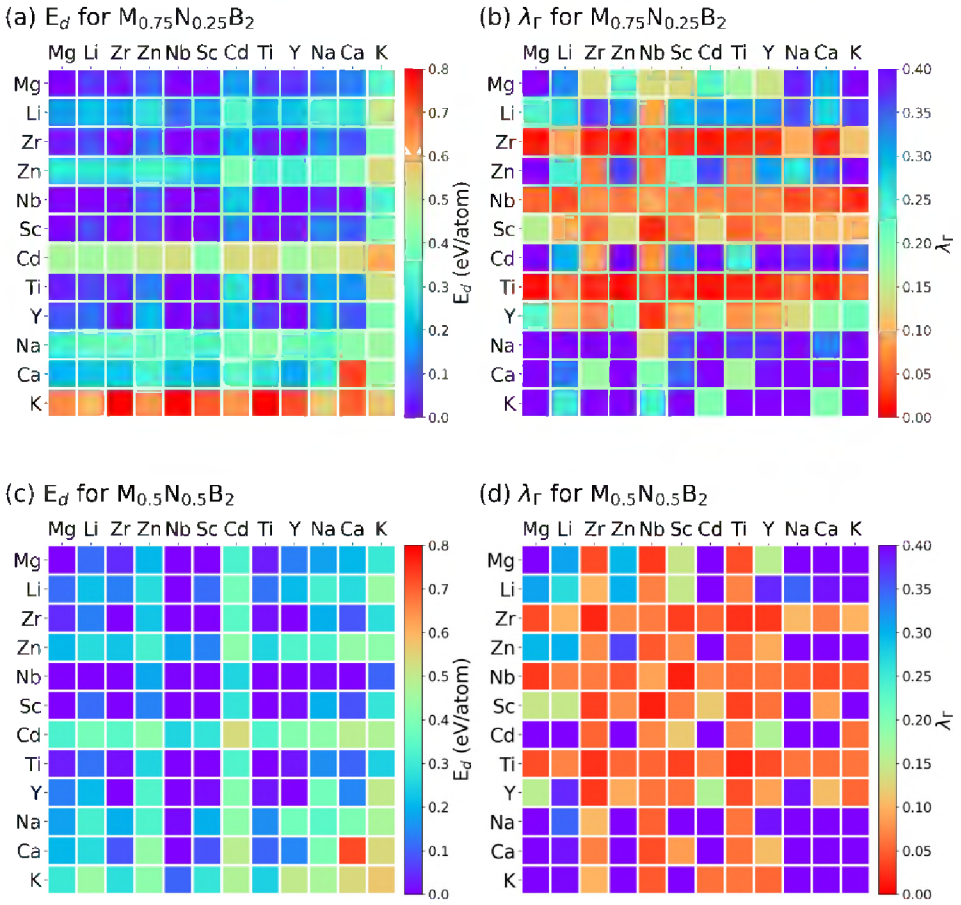

Figure 3 E_d and λ mapping of ternary metal diboride compounds. (a) and (b) are E_d and λ for $M_{0.75}N_{0.25}B_2$; (c) and (d) are E_d and λ for $M_{0.5}N_{0.5}B_2$. X axis indicates N site and Y axis indicates M site.

The E_d-λ_Γ correlation of all ternary phases are plotted in Fig. 4(a), which also shows a general trend of anti-correlation between stability and EPC strength, although the ternary data points appear to be more scattered than the binary ones shown in Fig. 1. To understand the cation mixing effect in ternary phases, we recalculate E_d and λ_Γ values by linearly interpolating between binary phases (e.g., $E_d(M_{1-x}N_xB_2) = (1-x)E_d(MB_2) + xE_d(NB_2)$), and compare the interpolated values with the real values in Fig. 4(b). E_d mostly follow the $y=x$ line, indicating insignificant mixing enthalpy for the ternary phases. However, λ_Γ in Fig. 4(b) strongly deviates from the $y=x$ line. A large group of ternary phases show a deteriorated λ_Γ compared to the linear combination of parent phases (blue line in Fig. 4(b)). Only a small group of ternary phases show an enhancement of λ_Γ due to the mixing (green line). This provides a qualitative explanation to many previously failed attempts at increasing T_c of MgB_2 by doping with other elements. Because the substitution has a much higher chance of deteriating, instead of enchancing, the EPC. Therefore, it is necessary to

perform a high-throughput screening of many substitution possibilities. We also checked the correlation between the density of states at Fermi level $N(\epsilon_F)$ and E_d or λ_Γ, and verified that $N(\epsilon_F)$ is not a dominant factor to fully describe the total energy and EPC.

A few ternary metal diborides containing Mg have been successfully synthesized previously [1, 13-18], as marked in Fig. 4. Table 1 lists detailed information on the doped $Mg_{1-x}N_xB_2$ that have been reported experimentally or calculated theoretically [1, 13-18, 25, 52-53]. One can see λ_Γ shows a consistent trend with the reported T_c values, indicating that the zone-center EPC calculation can reliably estimate the superconducting properties of this material family. It's important to note that experiments show that 20% of Zn, 10% of Na and 10% of Ca can be doped in the MgB_2 structure [15], while their E_d values are in the range of 0.1-0.2 eV/atom. Therefore, it provides a range of E_d to identify metastable phases that may be accessible in experiments. In Fig. 4, we use $E_d < 0.2$ eV/atom as the criteria to select structures with good stability. We use a threshold of $\lambda_\Gamma \sim 0.4$, (i.e. λ_Γ of MgB_2) to screen out structures with good EPC. The phases of interest that satisfy both criteria are located in the lower-right area of Fig.4 (a). While most phases in or near this area are the doped MgB_2, it also identifies three non-MgB_2 phases for further study, namely $NaScB_4$, Li_3ZrB_8 and Ca_3YB_8. By checking the full Brillouin zone phonon spectrum, we find $NaScB_4$ shows strong imaginary phonons (see Supplementary **Fig. S3**) while Li_3ZrB_8 and Ca_3YB_8 are dynamically stable. By analyzing the zone-center phonon modes, we find the EPCs in both systems are contributed by Raman-active E_{2g} modes, as shown in **Fig. S4**. These modes are two-dimensional on the boron layers, similar to the stretching modes in MgB_2, while the distributions on boron atoms are different (**Fig. S4**). It's interesting to note that λ_Γ of Li_3ZrB_8 is higher than those of LiB_2 and ZrB_2. Therefore, Li_3ZrB_8 can be an example of the enhanced EPC group due to the mixing (green line in Fig. 4(b)).

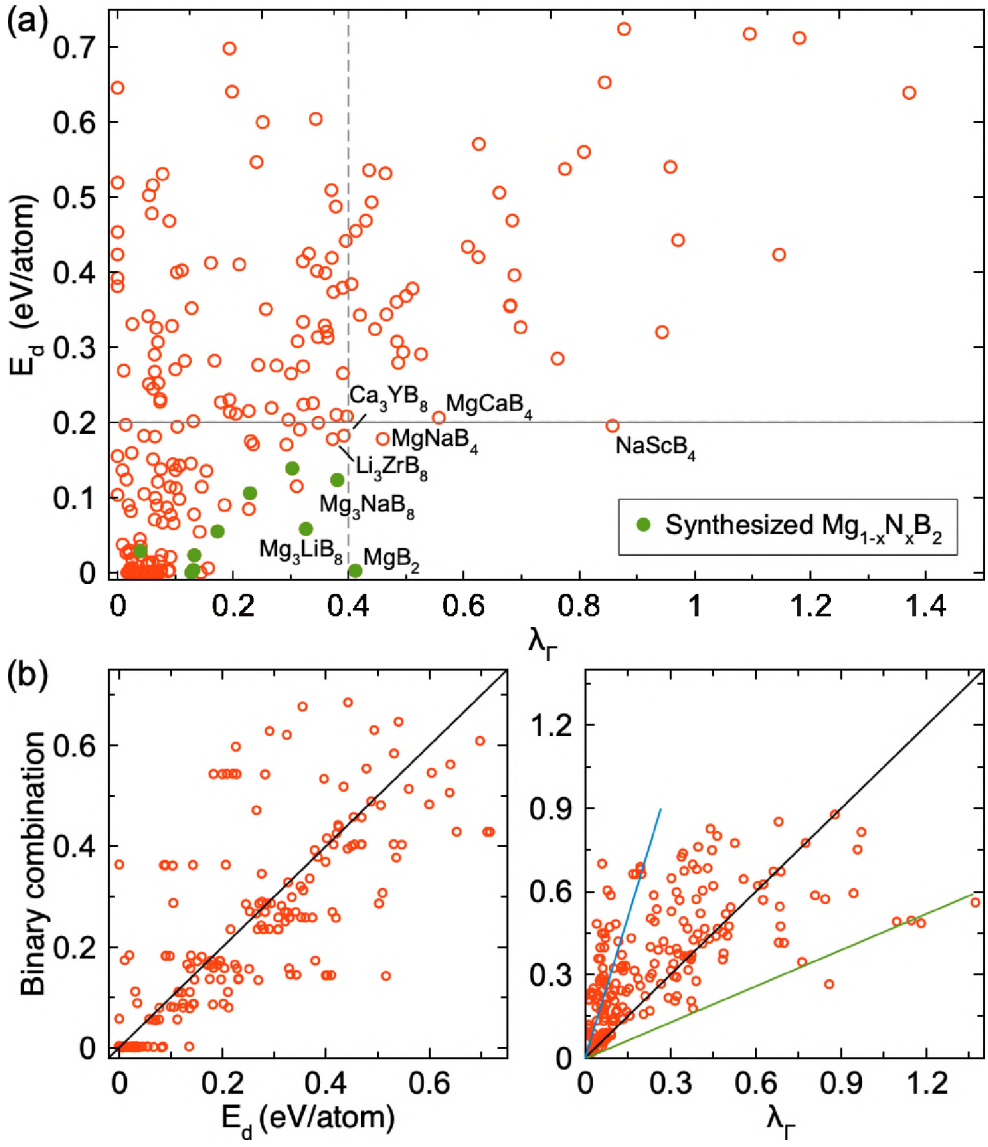

Figure 4 E_d and λ_Γ correlation in ternary metal diborides. (a) E_d-λ_Γ diagram for ternary $M_{1-x}N_xB_2$ structures. Green solid symbol indicates phases previously synthesized by experiments [1, 13-18]. The horizontal line indicates the range of synthesizable energetic stability. The vertical dashed line indicates λ_Γ value similar to MgB_2. (b) The comparison between the E_d (left panel) and λ_Γ (right panel) of ternary phases and the linear combinations of their binary counterparts. The x axis shows the value of ternary phases, i.e., $E_d(M_{1-x}N_xB_2)$ or $\lambda_\Gamma(M_{1-x}N_xB_2)$. The y axis shows the linear combination of the binary counterparts, i.e. $(1-x)E_d(MB_2) + xE_d(NB_2)$ or $(1-x)\lambda_\Gamma(MB_2) + x\lambda_\Gamma(NB_2)$. The black line indicates $y=x$ correlation. Blue and green lines indicate the deterioration and enhancement of λ_Γ, respectively.

Table 1. Zone-center EPC strength λ_Γ, previously calculated T_c or experimental T_c and energy above the convex hull E_d from present calculations for doped $Mg_{1-x}N_xB_2$ phases. The x in the bracket shows the previously studied composition.

$Mg_{1-x}N_xB_2$	λ_Γ	Calculated T_c (K)	Experimental T_c (K)	E_d (eV/atom)
MgB_2	0.41	42 [26]	39 [1]	0.0
$Mg_{0.75}Nb_{0.25}B_2$	0.13	-	39.3 (x=0.05) [16]	0.004
$Mg_{0.75}Li_{0.25}B_2$	0.33	31 (x=0.2) [52]	38.3 (x=0.3) [13]	0.058
$Mg_{0.75}Na_{0.25}B_2$	0.38	44-54 (x=0.2) [53]	38 (x=0.1) [15]	0.123
$Mg_{0.75}Ca_{0.25}B_2$	0.31	41-52 (x=0.2) [53]	38 (x=0.1) [15]	0.139
$Mg_{0.75}Zn_{0.25}B_2$	0.23	33 (x=0.2) [52]	38 (x=0.2) [15]	0.106
$Mg_{0.75}Zr_{0.25}B_2$	0.13	-	37.3 (x=0.2) [14]	0.023
$Mg_{0.75}Ti_{0.25}B_2$	0.18	25.5 [25]	30 (x=0.2) [18]	0.055
$Mg_{0.75}Sc_{0.25}B_2$	0.13	11.4 [25]	8.2 [17]	0.0
$Mg_{0.5}Ti_{0.5}B_2$	0.04	4.9 [25]	26 (x=0.4) [18]	0.029
$Mg_{0.5}Sc_{0.5}B_2$	0.15	8.8 [25]	-	0.003

3.4 Superconductivity in Li_3ZrB_8 and Ca_3YB_8

Because of promising synthesizability and EPC in Li_3ZrB_8 and Ca_3YB_8 phases, we perform DFPT calculations to compute the full Brioullion zone EPC constant and calculate T_c with McMillan equations (see Method). Fig. 5 shows the electronic structure and phonon spectrum for Li_3ZrB_8. The bands at the Fermi level are mainly from B's p electrons mixed with Zr's d electrons (Fig. 5(a)). Compared to the electronic structure of MgB_2 (Supplementary **Fig. S5**), the flat bands from Γ to A shows a cross at the Fermi level, which also results in a significant change in the Fermi surface in Fig. 5(b).

The phonon spectrum and density of the state of Li_3ZrB_8 are shown in Fig. 5(c). No imaginary-frequency modes are identified along the Brillouin zone's high-symmetry lines, indicating that Li_3ZrB_8 is dynamically stable. Three twofold degenerate E_{2g} modes of B atoms show strong EPC at the Γ point. This is consistent with the frozen-phonon analysis shown in Fig. 5. Unlike MgB_2 that the E_{2g} mode only shows EPC along the Γ-A line (Supplementary **Fig. S5**), the E_{2g} modes in Li_3ZrB_8 show EPC more evenly distributed in the Brillouin zone. This leads to an EPC constant λ = 1.04, much higher than the value of 0.62 for MgB_2 in the present calculation. The electronic and phonon analyses are also performed for Ca_3YB_8, as shown in Supplementary **Fig. S6**. The E_{2g} mode of Ca_3YB_8 shows EPC only along the Γ-A line, similar to MgB_2. The EPC constant of Ca_3YB_8 is λ = 0.64.

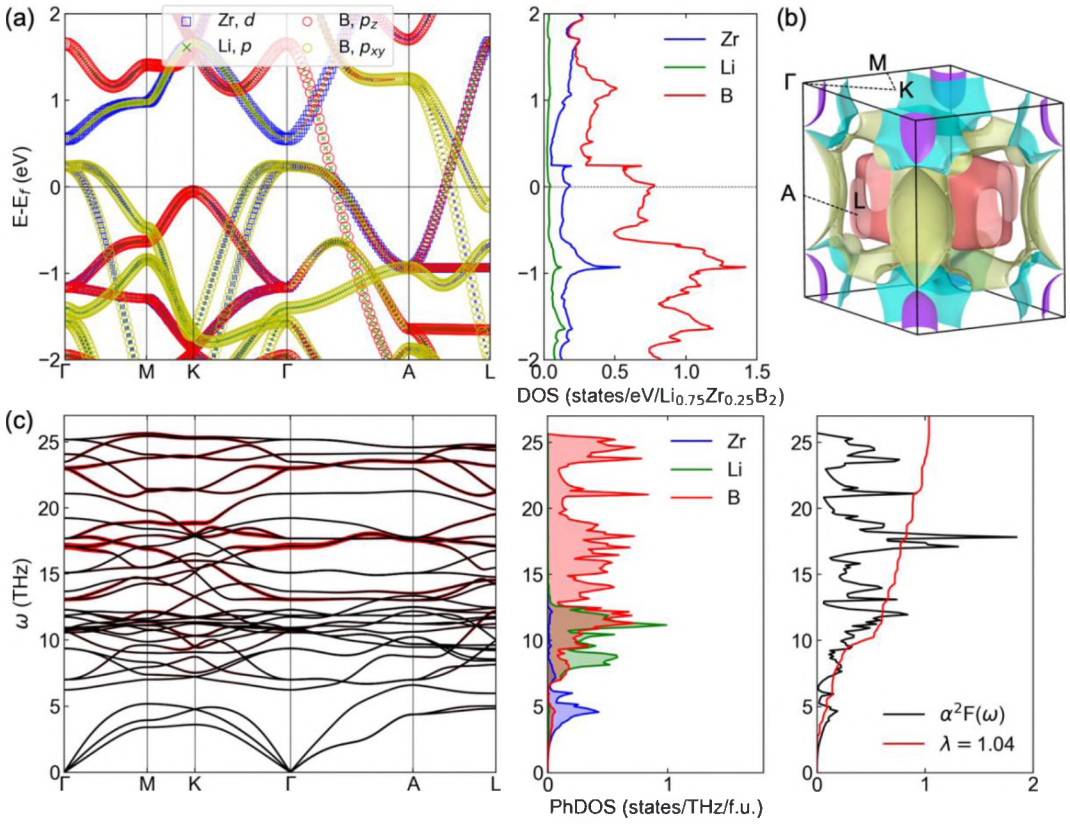

Figure 5 Electron structure and electron-phonon calculations for Li_3ZrB_8. (a) Electronic band structure and projected density of states. (b) Fermi surface. (c) Phonon dispersion, phonon density of state and Eliashberg spectrum. The red bands on the phonon dispersion indicate the strength of EPC.

We calculate T_c for Li_3ZrB_8 and Ca_3YB_8 with McMillan equations. We also re-calculate T_c for MgB_2 with the same method and same density of ***k***- and **q**-grid (see Method section). This provides us a reference to estimate T_c in the two ternary systems. For MgB_2, we obtain isotropic T_c = 19 K with the Allen-Dynes formula. This is consistent with the previous calculation (22 K in Ref.[6]) but underestimates the T_c compared to the experimental value of 39 K. The error is mainly due to the McMillan equation. One can improve it by employing a more sophisticated anisotropic Eliashberg theory [24] and Migdal-Eliashberg equation [54]. The non-adiabatic effects, which has been shown to be significant for MgB_2 and related system [55-57], may also be considered for ternary metal borides in future studies. Nevertheless, using the same accuracy, we obtain T_c as 38 K and 10 K for Li_3ZrB_8 and Ca_3YB_8, respectively. Therefore, the application of the McMillan formula for Li_3ZrB_8 produced T_c almost twice as larger than the one in MgB_2, while the T_c of Ca_3YB_8 is half of MgB_2.

IV. Conclusion

In summary, using first-principles high-throughput calculations, we search for ternary metal diborides with energetic stability and high EPC strength in 66 systems. 17 phases are identified to be stable ternary ground states and the ternary phase diagrams of these systems are updated accordingly. 78 metastable phases with E_d < 0.2 eV/atom are also identified. An anti-correlation between energetic stability and EPC

strength is revealed in both binary and ternary metal diborides. Two systems, Li_3ZrB_8 and Ca_3YB_8, show both good energetic stability and strong EPC strength. The T_c of Li_3ZrB_8 is predicted to be twice as large as that of MgB_2, calculated based on the McMillan formalism with the same parameters. The experimental verification of our prediction is highly desirable. Our studies demonstrate zone-center phonon calculations as an encouraging method for massive screening of multi-component systems for conventional high-T_c superconductors.

Acknowledgments

Work at Guangdong University of Technology was supported by the Guangdong Natural Science Foundation of China (Grant No. 2017B030306003, and No.2019B1515120078). R. Wang was supported by the Guangdong Basic and Applied Basic Research Foundation (Grant No. 2021A1515110328 & 2022A1515012174). F. Zheng, Y. Fang and S. Wu were supported by the National Natural Science Foundation of China (11874307). C.Z. Wang, V. Antropov and F. Zhang were supported by the U.S. Department of Energy (DOE), Office of Science, Basic Energy Sciences, Materials Science and Engineering Division. Ames Laboratory is operated for the U.S. DOE by Iowa State University under Contract No. DE-AC02-07CH11358, including the grant of computer time at the National Energy Research Supercomputing Center (NERSC) in Berkeley. Y. Sun was supported by National Science Foundation Awards No. DMR-2132666. R. Wang and H. Dong also thank Center of Campus Network and Modern Educational Technology of GDUT for providing computational resources and technical support for this work.

Supporting Information Available:

The structures of four symmetry-inequivalent crystal structures of M_3NB_8, MNB_4 and MN_3B_8 are shown in **Fig. S1**. DFT-calculated convex hull of 10 systems containing ternary ground stable phases are shown in **Fig. S2**. Phonon dispersion of $NaScB_4$ is shown in **Fig. S3**. Analysis of zone-center phonon and EPC from λ_Γ calculations for Li_3ZrB_8 and Ca_3YB_8 are shown in **Fig. S4**. Electron structure and electron-phonon calculations for MgB_2 are shown in **Fig. S5**. Electron structure and electron-phonon calculations for Ca_3YB_8 are shown in **Fig. S6**. The formation energies (E_f) and the formation energies above the convex hull (E_d) of ternary compounds which have E_d less than 0.2 eV/atom are shown in **Table S1**.

This information is available free of charge at the website: http://pubs.acs.org/

References

(1) Nagamatsu, J.; Nakagawa, N.; Muranaka, T.; Zenitani, Y.; Akimitsu, J., Superconductivity at 39 K in Magnesium Diboride. *Nature* **2001**, *410*, 63-64.

(2) Buzea, C.; Yamashita, T., Review of the Superconducting Properties of MgB_2. *Superconductor Science and Technology* **2001**, *14*, R115.

(3) Kortus, J.; Mazin, I. I.; Belashchenko, K. D.; Antropov, V. P.; Boyer, L. L., Superconductivity of Metallic Boron in MgB_2. *Physical Review Letters* **2001**, *86*, 4656-4659.

(4) Belashchenko, K. D.; Schilfgaarde, M. v.; Antropov, V. P., Coexistence of Covalent and Metallic Bonding in the Boron Intercalation Superconductor MgB_2. *Physical Review B* **2001**, *64*, 092503.

(5) An, J.; Pickett, W., Superconductivity of MgB_2: Covalent Bonds Driven Metallic. *Physical Review Letters* **2001**, *86*, 4366.

(6) Liu, A. Y.; Mazin, I. I.; Kortus, J., Beyond Eliashberg Superconductivity in MgB_2: Anharmonicity, Two-Phonon Scattering, and Multiple Gaps. *Physical Review Letters* **2001**, *87*, 087005.

(7) Kong, Y.; Dolgov, O.; Jepsen, O.; Andersen, O., Electron-Phonon Interaction in the Normal and Superconducting States of MgB_2. *Physical Review B* **2001**, *64*, 020501.

(8) Choi, H. J.; Roundy, D.; Sun, H.; Cohen, M. L.; Louie, S. G., First-Principles Calculation of the Superconducting Transition in MgB_2 within the Anisotropic Eliashberg Formalism. *Physical Review B* **2002**, *66*, 020513.

(9) Mazin, I. I.; Antropov, V. P., Electronic Structure, Electron–Phonon Coupling, and Multiband Effects in MgB_2. *Physica C: Superconductivity* **2003**, *385*, 49-65.

(10) Cava, R. J.; Zandbergen, H. W.; Inumaru, K., The Substitutional Chemistry of MgB_2. *Physica C: Superconductivity* **2003**, *385*, 8-15.

(11) Karpinski, J.; Zhigadlo, N. D.; Katrych, S.; Puzniak, R.; Rogacki, K.; Gonnelli, R., Single Crystals of MgB_2: Synthesis, Substitutions and Properties. *Physica C: Superconductivity* **2007**, *456*, 3-13.

(12) Karpinski, J.; Zhigadlo, N.; Katrych, S.; Rogacki, K.; Batlogg, B.; Tortello, M.; Puzniak, R., MgB_2 Single Crystals Substituted with Li and with Li-C: Structural and Superconducting Properties. *Physical Review B* **2008**, *77*, 214507.

(13) Pallecchi, I., et al., Investigation of Li-Doped MgB_2. *Superconductor Science and Technology* **2009**, *22*, 095014.

(14) Feng, Y.; Zhao, Y.; Pradhan, A. K.; Cheng, C. H.; Yau, J. K. F.; Zhou, L.; Koshizuka, N.; Murakami, M., Enhanced Flux Pinning in Zr-Doped MgB_2 Bulk Superconductors Prepared at Ambient Pressure. *Journal of Applied Physics* **2002**, *92*, 2614-2619.

(15) Toulemonde, P.; Musolino, N.; Flükiger, R., High-Pressure Synthesis of Pure and Doped Superconducting MgB_2 Compounds. *Superconductor Science and Technology* **2003**, *16*, 231.

(16) Kalavathi, S.; Divakar, C., Superconductivity in Dense $Mg_{1-x}M_xB_2$ (M= Zr, Nb, Mo; x= 0.05) Materials Sintered under Pressure. *Bulletin of Materials Science* **2005**, *28*, 249-252.

(17) Agrestini, S.; Metallo, C.; Filippi, M.; Simonelli, L.; Campi, G.; Sanipoli, C.; Liarokapis, E.; De Negri, S.; Giovannini, M.; Saccone, A., Substitution of Sc for Mg in MgB_2: Effects on Transition Temperature and Kohn Anomaly. *Physical Review B* **2004**, *70*, 134514.

(18) Lee, B. W.; Choi, I.; Jung, C. U.; Lee, S. I., Doping in MgB_2 Superconductors Using a High-Pressure Furnace. *Journal of Magnetism and Magnetic Materials* **2008**, *320*, e484-e486.

(19) Gasparov, V. A.; Sidorov, N.; Zver'Kova, I.; Kulakov, M., Electron Transport in Diborides: Observation of Superconductivity in ZrB_2. *Journal of Experimental and Theoretical Physics Letters* **2001**, *73*, 532-535.

(20) Leyarovska, L.; Leyarovski, E., A Search for Superconductivity Below 1 K in Transition Metal Borides. *Journal of the Less Common Metals* **1979**, *67*, 249-255.

(21) Rosner, H.; Pickett, W.; Drechsler, S.-L.; Handstein, A.; Behr, G.; Fuchs, G.; Nenkov, K.;

Müller, K.-H.; Eschrig, H., Electronic Structure and Weak Electron-Phonon Coupling in TaB_2. *Physical Review B* **2001**, *64*, 144516.

(22) Pei, C.; Zhang, J.; Wang, Q.; Zhao, Y.; Gao, L.; Gong, C.; Tian, S.; Luo, R.; Lu, Z.-Y.; Lei, H., Pressure-Induced Superconductivity at 32 K in MoB_2. *arXiv preprint arXiv:2105.13250* **2021**.

(23) Lim, J., et al., Creating Superconductivity in WB_2 through Pressure-Induced Metastable Planar Defects. *arXiv preprint arXiv:2109.11521* **2021**.

(24) Choi, H. J.; Louie, S. G.; Cohen, M. L., Prediction of Superconducting Properties of CaB_2 Using Anisotropic Eliashberg Theory. *Physical Review B* **2009**, *80*, 064503.

(25) Mackinnon, I. D. R.; Talbot, P. C.; Alarco, J. A., Phonon Dispersion Anomalies and Superconductivity in Metal Substituted MgB_2. *Computational Materials Science* **2017**, *130*, 191-203.

(26) Alarco, J. A.; Talbot, P. C.; Mackinnon, I. D., Phonon Anomalies Predict Superconducting T_c for AlB_2-Type Structures. *Physical Chemistry Chemical Physics* **2015**, *17*, 25090-25099.

(27) Baroni, S.; de Gironcoli, S.; Dal Corso, A.; Giannozzi, P., Phonons and Related Crystal Properties from Density-Functional Perturbation Theory. *Reviews of Modern Physics* **2001**, *73*, 515-562.

(28) Sun, Y.; Zhang, F.; Wang, C.-Z.; Ho, K.-M.; Mazin, I. I.; Antropov, V., Electron-Phonon Coupling Strength from *ab initio* Frozen-Phonon Approach. *Physical Review Materials* **2022**, *6*, 074801.

(29) Blöchl, P. E., Projector Augmented-Wave Method. *Physical Review B* **1994**, *50*, 17953-17979.

(30) Kresse, G.; Furthmüller, J., Efficiency of Ab-Initio Total Energy Calculations for Metals and Semiconductors Using a Plane-Wave Basis Set. *Computational Materials Science* **1996**, *6*, 15-50.

(31) Kresse, G.; Furthmüller, J., Efficient Iterative Schemes for *ab initio* Total-Energy Calculations Using a Plane-Wave Basis Set. *Physical Review B* **1996**, *54*, 11169-11186.

(32) Perdew, J. P.; Burke, K.; Ernzerhof, M., Generalized Gradient Approximation Made Simple. *Physical Review Letters* **1996**, *77*, 3865-3868.

(33) Monkhorst, H. J.; Pack, J. D., Special Points for Brillouin-Zone Integrations. *Physical Review B* **1976**, *13*, 5188-5192.

(34) Jain, A., et al., Commentary: The Materials Project: A Materials Genome Approach to Accelerating Materials Innovation. *APL Materials* **2013**, *1*, 011002.

(35) Togo, A.; Tanaka, I., First Principles Phonon Calculations in Materials Science. *Scripta Materialia* **2015**, *108*, 1-5.

(36) Giannozzi, P.; Baroni, S.; Bonini, N.; Calandra, M.; Car, R.; Cavazzoni, C.; Ceresoli, D.; Chiarotti, G. L.; Cococcioni, M.; Dabo, I., Quantum Espresso: A Modular and Open-Source Software Project for Quantum Simulations of Materials. *Journal of physics: Condensed matter* **2009**, *21*, 395502.

(37) Giannozzi, P.; Andreussi, O.; Brumme, T.; Bunau, O.; Nardelli, M. B.; Calandra, M.; Car, R.; Cavazzoni, C.; Ceresoli, D.; Cococcioni, M., Advanced Capabilities for Materials Modelling with Quantum Espresso. *Journal of physics: Condensed matter* **2017**, *29*, 465901.

(38) Giannozzi, P., et al., Quantum Espresso toward the Exascale. *The Journal of Chemical Physics* **2020**, *152*, 154105.

(39) Garrity, K. F.; Bennett, J. W.; Rabe, K. M.; Vanderbilt, D., Pseudopotentials for High-Throughput DFT Calculations. *Computational Materials Science* **2014**, *81*, 446-452.

(40) Eliashberg, G., Interactions between Electrons and Lattice Vibrations in a Superconductor. *Sov. Phys. JETP* **1960**, *11*, 696-702.

(41) McMillan, W., Transition Temperature of Strong-Coupled Superconductors. *Physical Review* **1968**, *167*, 331.

(42) Allen, P. B., Neutron Spectroscopy of Superconductors. *Physical Review B* **1972**, *6*, 2577.

(43) Allen, P. B.; Dynes, R., Transition Temperature of Strong-Coupled Superconductors Reanalyzed. *Physical Review B* **1975**, *12*, 905.

(44) Akarsu, M. K.; Akin, I., Effects of Graphene Nanoplatelets and Hexagonal Boron Nitride on Spark Plasma Sintered (Zr,Nb)B_2 Solid Solutions. *Journal of Alloys and Compounds* **2021**, *884*, 161110.

(45) Bhaskar, G.; Gvozdetskyi, V.; Batuk, M.; Wiaderek, K. M.; Sun, Y.; Wang, R.; Zhang, C.; Carnahan, S. L.; Wu, X.; Ribeiro, R. A., Topochemical Deintercalation of Li from Layered LiNiB: Toward 2D MBene. *Journal of the American Chemical Society* **2021**, *143*, 4213-4223.

(46) Bikowski, A.; Siol, S.; Gu, J.; Holder, A.; Mangum, J. S.; Gorman, B.; Tumas, W.; Lany, S.; Zakutayev, A., Design of Metastable Tin Titanium Nitride Semiconductor Alloys. *Chemistry of Materials* **2017**, *29*, 6511-6517.

(47) Arca, E., et al., Redox-Mediated Stabilization in Zinc Molybdenum Nitrides. *Journal of the American Chemical Society* **2018**, *140*, 4293-4301.

(48) Oganov, A. R.; Glass, C. W., Crystal Structure Prediction Using *ab initio* Evolutionary Techniques: Principles and Applications. *The Journal of Chemical Physics* **2006**, *124*, 244704.

(49) Wang, Y.; Lv, J.; Zhu, L.; Ma, Y., Crystal Structure Prediction Via Particle-Swarm Optimization. *Physical Review B* **2010**, *82*, 094116.

(50) Zhao, X., et al., Exploring the Structural Complexity of Intermetallic Compounds by an Adaptive Genetic Algorithm. *Physical Review Letters* **2014**, *112*, 045502.

(51) Wu, S.; Ji, M.; Wang, C.-Z.; Nguyen, M. C.; Zhao, X.; Umemoto, K.; Wentzcovitch, R.; Ho, K.-M., An Adaptive Genetic Algorithm for Crystal Structure Prediction. *Journal of Physics: Condensed Matter* **2013**, *26*, 035402.

(52) Singh, P., Theoretical Study of Superconductivity in MgB_2 and Its Alloys. *Bulletin of Materials Science* **2003**, *26*, 131-135.

(53) Neaton, J.; Perali, A., On the Possibility of Superconductivity at Higher Temperatures in

Sp-Valent Diborides. *arXiv preprint cond-mat/0104098* **2001**.

(54) Margine, E. R.; Giustino, F., Anisotropic Migdal-Eliashberg Theory Using Wannier Functions. *Physical Review B* **2013**, *87*, 024505.

(55) Alexandrov, A. S., Nonadiabatic Polaronic Superconductivity in MgB_2 and Cuprates. *Physica C: Superconductivity* **2001**, *363*, 231-236.

(56) Cappelluti, E.; Ciuchi, S.; Grimaldi, C.; Pietronero, L.; Strässler, S., High T_c Superconductivity in MgB_2 by Nonadiabatic Pairing. *Physical Review Letters* **2002**, *88*, 117003.

(57) Szczęśniak, D.; Szczęśniak, R., Signatures of Nonadiabatic Superconductivity in Lithium-Decorated Graphene. *Physical Review B* **2019**, *99*, 224512.

Table of Contents Graphic

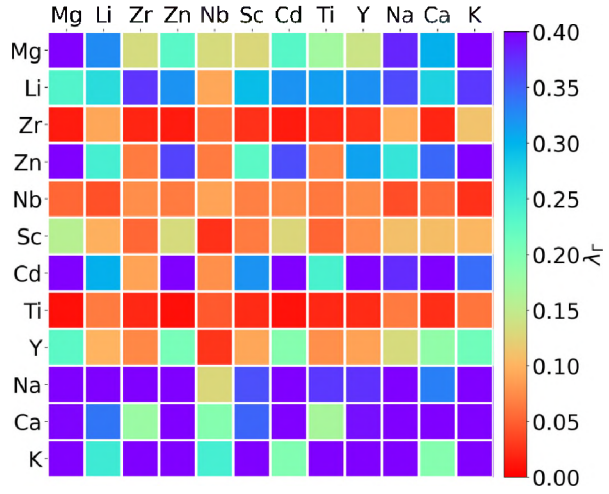

Synopsis

We perform a high-throughput screening on phonon-mediated superconductivity in ternary metal diboride structure with alkali, alkaline earth, and transition metals. From fast calculations of zone-center electron-phonon coupling, 43 compounds are revealed to show electron-phonon coupling strength higher than that of MgB_2. Li_3ZrB_8 and Ca_3YB_8 show reasonable energetic stability and superconducting T_c.